Floquet Dynamics in Driven Fermi-Hubbard Systems

Michael Messer, Kilian Sandholzer, Frederik Görg, Joaquín Minguzzi, Rémi Desbuquois, and Tilman Esslinger
Institute for Quantum Electronics, ETH Zurich, 8093 Zurich, Switzerland

(Received 31 July 2018; published 7 December 2018)

We study the dynamics and timescales of a periodically driven Fermi-Hubbard model in a three-dimensional hexagonal lattice. The evolution of the Floquet many-body state is analyzed by comparing it to an equivalent implementation in undriven systems. The dynamics of double occupancies for the near- and off-resonant driving regime indicate that the effective Hamiltonian picture is valid for several orders of magnitude in modulation time. Furthermore, we show that driving a hexagonal lattice compared to a simple cubic lattice allows us to modulate the system up to 1 s, corresponding to hundreds of tunneling times, with only minor atom loss. Here, driving at a frequency close to the interaction energy does not introduce resonant features to the atom loss.

DOI: 10.1103/PhysRevLett.121.233603

Floquet engineering is a versatile method for implementing novel, effectively static Hamiltonians by applying a periodic drive to a quantum system [1–3]. For long timescales, a limitation for this method to create interesting many-body states is the eventual heating to an infinite temperature, caused by the presence of integrability breaking terms such as interactions [4,5]. For very short timescales, an obvious limit is set by the duration of a single cycle, which cannot be captured by a static Hamiltonian. In general, the launch of the drive causes complex dynamics on different timescales in a many-body system [6–8]. Theoretical considerations suggest that an effective Hamiltonian picture can still remain valid for some intermediate timescale required to create many-body phases [7,9–17]. Thus, developing an experimental approach to identify relevant timescales in a periodically driven quantum system with interactions is a timely challenge.

In this Letter, we investigate the Floquet dynamics of a periodically driven Fermi-Hubbard model, which is realized with interacting fermions in a three-dimensional optical lattice. Our approach allows us to experimentally compare the evolution of an observable in a driven system with the equivalent dynamics in an undriven Hamiltonian. The evolution of the entire many-body state is complex [see Fig. 1(a)]—while local processes, like tunneling, play a role on short timescales, the trapping potential sets a timescale for global thermalization. In addition, deviations to the expected behavior in the effective Hamiltonian might arise for very long modulation times. In the comparison, we analyze this evolution of the many-body state due to a change of (effective) Hubbard parameters and disentangle it from heating in driven systems which cannot be captured by an effective static model. The latter can be understood as unwanted absorption processes, which in the presence of interactions, may be resonant at any driving frequency, since the energy spectrum becomes continuous [18–21]. Although resonant processes can be desired to realize a specific Floquet Hamiltonian [22–35], a general understanding of the dynamics of strongly correlated driven quantum states over several orders of magnitude in evolution time remains challenging [17,36–40].

For our measurements, we prepare a degenerate fermionic cloud with $N = 38(4) \times 10^3$ interacting, ultracold ^{40}K atoms equally populating two magnetic sublevels of the $F = 9/2$ hyperfine manifold at a temperature of 10(1)% of the Fermi temperature. The atoms are then loaded into the lowest band of a three-dimensional optical lattice with hexagonal geometry [41]. The hexagonal lattice in the xz plane is a bipartite lattice with sublattices $\mathcal{A}$ and $\mathcal{B}$ and is stacked along the y direction [see Fig. 1(b) and [42]]. The position of the retroreflecting lattice mirror along the x direction is, then, periodically modulated using a piezoelectric actuator at frequency $\omega/(2\pi)$ and an independently calibrated amplitude A. To compare the evolution of the many-body state under the driven and undriven Hamiltonian, we measure the fraction of doubly occupied sites $\mathcal{D}$ for different times, by performing an interaction dependent rf spectroscopy [42]. Since $\mathcal{D}$ is directly influenced by the interplay of the interactions and tunneling (U/t), it serves as a direct probe of the many-body state. For example, at equal filling, a Mott insulating state ($U \gg t$) is depicted by a negligible $\mathcal{D}$, while it is increased for metallic states [43,44].

For an off-resonant modulation, where the driving frequency is the dominant energy scale ($\hbar\omega \gg U,\ t$), our system is described by the effective Hamiltonian [33,45–47]

$$\hat{H}^{\mathrm{eff}}_{\text{off-res}} = -t_x \mathcal{J}_0(K_0) \sum_{\langle i,j\rangle_x,\sigma} \hat{c}^\dagger_{i\sigma}\hat{c}_{j\sigma} - t_{y,z} \sum_{\langle i,j\rangle_{y,z},\sigma} \hat{c}^\dagger_{i\sigma}\hat{c}_{j\sigma} + U\sum_i \hat{n}_{i\downarrow}\hat{n}_{i\uparrow} + \sum_i V_i \hat{n}_i, \quad (1)$$

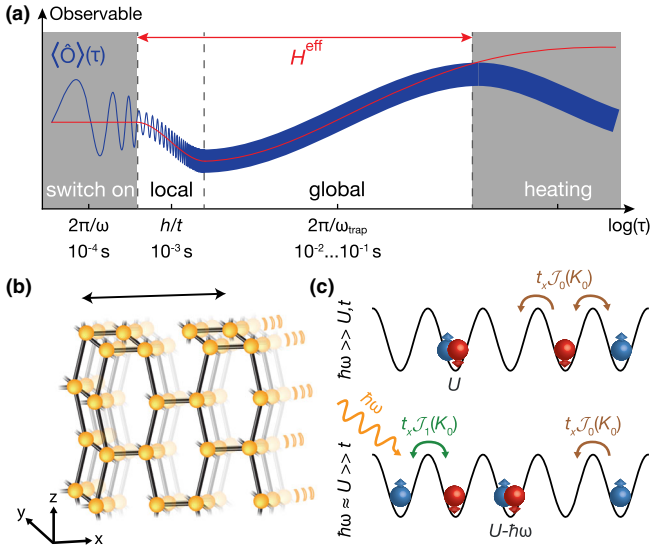

FIG. 1. Periodically driven Fermi-Hubbard model. (a) Altering the effective Hamiltonian (H^{eff}) affects the underlying many-body state and results in a change of the measured observable within different timescales of the system. A full time evolution of the observable is depicted in blue, while the time evolution under H^{eff} is plotted in red. Deviations to the expected behavior in the effective Hamiltonian can arise for long modulation times when heating processes dominate. (b) Three-dimensional hexagonal structure to realize the driven Fermi-Hubbard model. (c) Schematics of the tight-binding model of the effective Hamiltonian. For off-resonant driving ($\hbar\omega \gg U,\ t$), the interactions U are unaffected while the tunneling t is renormalized. In contrast, for near-resonant driving ($\hbar\omega \approx U \gg t$), the system exhibits a reduced effective interaction and a density assisted hopping process which is different from the single particle hopping.

where $\hat{c}^{\dagger}_{i\sigma}$ ($\hat{c}_{i\sigma}$) are the creation (annihilation) operators of one fermion with spin $\sigma = \uparrow, \downarrow$ at lattice site i and $\hat{n}_{i\sigma} = \hat{c}^{\dagger}_{i\sigma}\hat{c}_{i\sigma}$. The tunneling rates $t_{x,y,z}$ connect nearest neighbors $\langle i, j\rangle$ along x, y, z, and U is the on-site interaction energy. The last term represents the harmonic confinement of the trap, characterized by the mean trapping frequency $\bar{\omega}$ [42]. In the off-resonant regime, the tunneling energy along the driving direction (x) is renormalized by the zeroth-order Bessel function $\mathcal{J}_0$ with the dimensionless driving amplitude $K_0 = mA\omega d_x/\hbar$ in the argument, where m is the mass and d_x the lattice spacing [48].

When we modulate near resonantly to the interaction energy ($\hbar\omega \approx U \gg t$), the effective Hamiltonian is to lowest order in $1/\omega$ given by [25,33,49,50]

$$\hat{H}^{\mathrm{eff}}_{\mathrm{res}} = -\sum_{\langle i,j\rangle_x,\sigma}\left(t_x^{\mathrm{eff},0}\hat{g}_{ij\bar{\sigma}} + t_x^{\mathrm{eff},D}[\hat{h}^{\dagger}_{ij\bar{\sigma}} + \mathrm{H.c.}]\right) - t_{y,z}\sum_{\langle i,j\rangle_{y,z},\sigma}\hat{g}_{ij\bar{\sigma}} + (U-\hbar\omega)\sum_i \hat{n}_{i\downarrow}\hat{n}_{i\uparrow} + \sum_i V_i\hat{n}_i. \tag{2}$$

Here, the interaction is effectively modified to a value $U^{\mathrm{eff}} = U - \hbar\omega$. This can be understood as the exchange of photons with the drive. In addition, we have to differentiate between tunneling events which keep the number of double occupancies constant [$t_x^{\mathrm{eff},0}$ with $\hat{g}_{ij\bar{\sigma}} = (1-\hat{n}_{i\bar{\sigma}})\hat{c}^{\dagger}_{i\sigma}\hat{c}_{j\sigma}(1-\hat{n}_{j\bar{\sigma}}) + \hat{n}_{i\bar{\sigma}}\hat{c}^{\dagger}_{i\sigma}\hat{c}_{j\sigma}\hat{n}_{j\bar{\sigma}}$ and $\bar{\uparrow} = \downarrow$] and those which increase or decrease it by one unit [$t_x^{\mathrm{eff},D}$ with $\hat{h}^{\dagger}_{ij\bar{\sigma}} = \pm\hat{n}_{i\bar{\sigma}}\hat{c}^{\dagger}_{i\sigma}\hat{c}_{j\sigma}(1-\hat{n}_{j\bar{\sigma}})$, where the positive sign is valid for $i < j$ and vice versa]. The tunneling of a particle to an empty neighboring site is unaffected by the interaction resonance, and we obtain $t_x^{\mathrm{eff},0} = t_x\mathcal{J}_0(K_0)$, as in the off-resonant case. In contrast, if a double occupancy is involved in the tunneling process, we get $t_x^{\mathrm{eff},D} = t_x\mathcal{J}_1(K_0)$, thereby realizing density assisted tunneling processes [24,27–31,33,51,52]. Figure 1(c) presents a schematic overview of the microscopic processes for the off- and near-resonant drives.

In a first set of measurements, we compare the evolution of the fraction of doubly occupied sites ($\mathcal{D} = 2/N\sum_i\langle\hat{n}_{i\downarrow}\hat{n}_{i\uparrow}\rangle$) under a change of the Hamiltonian for off-resonant modulation and an equivalent ramp in the undriven system. We load a honeycomb lattice with $[t_{x,y,z}/h = (200(30), 40(3), 40(3))$ Hz] at $U/h = 500(30)$ Hz and linearly ramp up the amplitude $K_0 = 1.69(2)$ at a modulation frequency $\omega/(2\pi) = 7.25$ kHz within a variable ramp time τ_{ramp} [see Fig. 2(a)]. After the modulation ramp is completed, the tunneling in x is reduced to $t_x^{\mathrm{eff}} = t_x\mathcal{J}_0(K_0) \approx 0.4t_x$. We achieve the same final t_x by linearly ramping the lattice depth of an undriven system. Interestingly, the measured $\mathcal{D}$ in the driven system follows the results of the undriven lattice for all timescales. Both data sets can be compared to the evolution of the initial (black) and final lattice (orange), which is reached within 1 ms. We can explain this effect with a local change of the population of double occupancies and single particles due to an increased U/t_x^{eff}. A similar behavior has been observed with nearest-neighbor spin correlations in a driven honeycomb lattice for a fixed ramp time [33]. Already, a single driving cycle reduces the level of $\mathcal{D}$, indicating that the effective Hamiltonian picture can be valid on such short timescales [53].

To focus on the global timescales, we use a lattice with faster tunneling $[t_{x,y,z}/h = (510(90), 100(6), 100(10))$ Hz] and, first, ramp up the driving within 5 ms, which we have observed is adiabatic with respect to local timescales [42]. At maximal amplitude of $K_0 = 1.69(3)$, $U/h = 700(20)$ Hz, and a driving frequency of 4.25 kHz, we vary the modulation time τ_{hold} and compare the resulting change of $\mathcal{D}$ with a ramp in the undriven lattice [see Fig. 2(b)]. We observe a slowly increasing $\mathcal{D}$, as expected from the density redistribution caused by an increased μ/t. Both measurements follow each other up to $\tau_{\mathrm{hold}} = 50$ ms, which corresponds to more than 200 driving cycles. As a result, even at timescales where the trap redistribution plays a role ($\bar{\omega}/2\pi = 85.2(8)$ Hz), the off-resonantly modulated

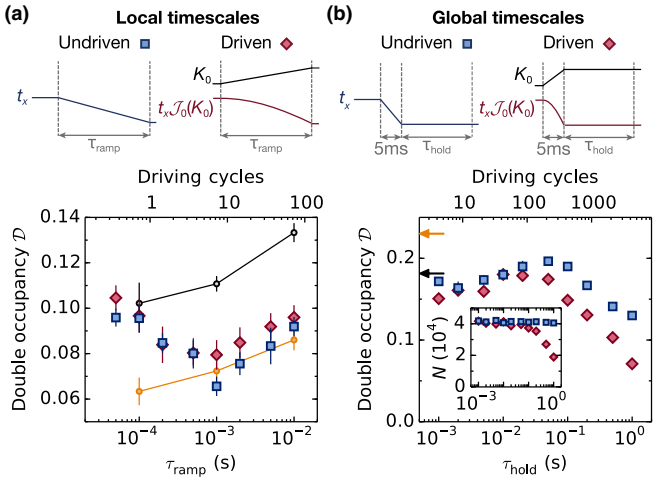

FIG. 2. Off-resonantly modulated Fermi-Hubbard model. (a) Starting from a $[t_{x,y,z}/h = (200(30), 40(3), 40(3))$ Hz] hexagonal lattice, we either increase the driving amplitude to $K_0 = 1.69(2)$ or perform a lattice ramp (undriven lattice) to imitate the same final $t_x/h = t_x^{\rm eff}/h = 80(10)$ Hz. The evolution of double occupancy fraction $\mathcal{D}$ on a local timescale for the driven (red diamonds) and undriven lattices (blue squares) as a function of the ramp-up time $\tau_{\rm ramp}$ at $U/h = 500(30)$ Hz. Evolution of $\mathcal{D}$ when loading directly into the starting (final) lattice is shown in black (orange) circles. (b) For the global timescales, we start with a $[t_{x,y,z}/h = (510(90), 100(6), 100(10))$ Hz] lattice and ramp up the drive within 5 ms or directly decrease t_x to $t_x^{\rm eff}/h = 210(40)$ Hz. Measured $\mathcal{D}$ at $U/h = 700(20)$ Hz as a function of the modulation time $\tau_{\rm hold}$ at constant $K_0 = 1.69(3)$ (red diamonds) and its counterpart in the undriven case (blue squares). Arrows indicating the reference values in the starting (final) lattice are shown in black (orange). The inset shows the corresponding number of atoms N as a function of $\tau_{\rm hold}$. Data points in a(b) are the mean and standard error of 5(10) individual measurements at different times within one driving period (see [42]).

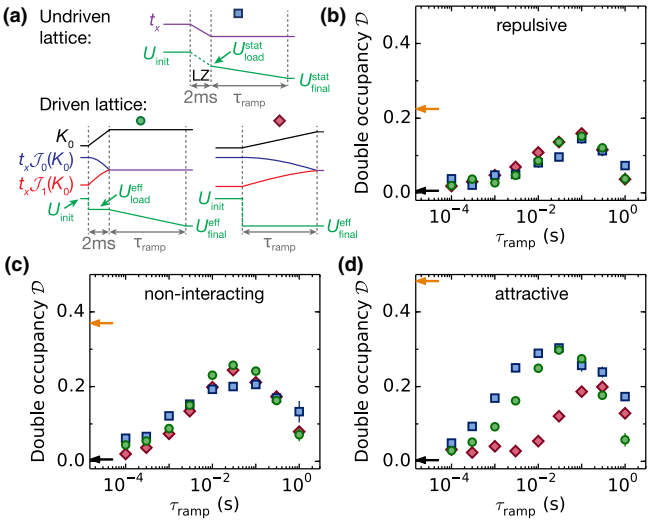

FIG. 3. Near-resonantly modulated Fermi-Hubbard model. (a) In the undriven lattice (blue squares) we change $U^{\rm stat}$ in 2 ms using a Landau-Zener (LZ) transfer to a different spin state and, also, lower t_x. For near-resonant driving, we either increase K_0 to 1.43(2) on a fixed timescale (2 ms) at $U_{\rm load}/h = 4.63(10)$ kHz and, then, tune the interactions in the driven system within a variable time $\tau_{\rm ramp}$ (green circles), or we, first, prepare the system at the final interaction $U_{\rm final}$ and, then, vary $\tau_{\rm ramp}$ of the K_0 ramp (red diamonds). (b)–(d) Dynamics of $\mathcal{D}$ for different $\tau_{\rm ramp}$ and three values of the final effective interaction $U_{\rm final}^{\rm eff}/h = [0.69(8), -0.02(6), -0.72(5)]$ kHz or the corresponding static counterpart $U^{\rm stat}$. Arrows indicate the reference values when adiabatically loading the atoms in the starting lattice $[t_{x,y,z}/h = (200(30), 100(10), 100(10))$ Hz] (black) or the final lattice with reduced tunneling $t_x^{\rm eff}/h = 110(20)$ Hz and $U^{\rm eff}$ (orange). Data points are the mean and standard error of five individual measurements at different times within one driving period [42].

Fermi-Hubbard model is captured by the effective Hamiltonian in Eq. (1). For $\tau_{\rm hold} > 0.1$ s we observe a decrease of $\mathcal{D}$, even in the undriven case, which we attribute to technical heating for a trapped system at intermediate interactions [43]. In both cases, this heating prevents a full redistribution of density in the trap as the adiabatic reference value is not fully reached (orange arrow). On a similar timescale, the driven lattice exhibits a loss of atoms [see inset of Fig. 2(b)] which will be analyzed in more detail in Fig. 4.

In a second set of measurements, we probe the validity of the effective Hamiltonian for a near-resonant modulation ($\hbar\omega \approx U \gg t$). In contrast to the measurements so far, we prepare our initial system in a Mott insulating state ($U_{\rm init}/h > 4.6(1)$ kHz) with negligible $\mathcal{D}$ and follow two different driving protocols at fixed $\omega/(2\pi) = 3.5$ kHz [see Fig. 3(a)]. We choose $K_0 = 1.43(2)$ such that tunneling is independent of the density [$\mathcal{J}_0(K_0) = \mathcal{J}_1(K_0)$, see Eq. (2)] which allows us to compare the system to an undriven parameter ramp. We either switch on K_0 to its maximal value within a variable time $\tau_{\rm ramp}$ at the final interaction $U_{\rm final}$ (red diamonds), or we follow a more intricate protocol. For this, we first ramp up K_0 in 2 ms at $U_{\rm load}$ detuned from resonance and, then, adjust $U_{\rm load} \to U_{\rm final}$ (via a Feshbach resonance) while modulating [42]. For both modulation protocols, the effective interaction is renormalized accordingly (e.g., $U_{\rm final}^{\rm eff} = U_{\rm final} - \hbar\omega$).

For comparison, in an undriven lattice, we need to ramp t_x to mimic the renormalized tunneling and additionally ramp the interactions $U^{\rm stat}$ [see Fig. 3(a)]. The latter is achieved by using the Feshbach resonances of two different spin mixtures, which have different values of $U^{\rm stat}$ at a fixed magnetic field. Hence, we perform a Landau-Zener transfer between two internal spin states, thereby reducing the initial strong repulsive interactions to weakly repulsive values within 2 ms [42]. In a final step, we ramp the magnetic field on a variable time to mimic $U^{\rm stat} = U^{\rm eff}$.

The dynamics of $\mathcal{D}$ as a function of $\tau_{\rm ramp}$ are shown in Fig. 3. We choose three different detunings $U_{\rm final} - \hbar\omega$

which result in a weakly repulsive, noninteracting for a modulation on resonance, and weakly attractive effective interaction. In all measurements, $\mathcal{D}$ initially increases since the Mott insulating regime is altered by the reduced effective interactions, but does not reach the reference value when adiabatically loading a weakly interacting cloud. Both the weakly repulsive and the noninteracting cases do not show a difference in $\mathcal{D}$ for the two modulation protocols and follow the expectation of the undriven system.

However, for effective attractive interactions, we observe a strong deviation. Here, the system is sensitive to the ramping protocol although all schemes reach the same final Hubbard parameters. For near-resonant driving, measurements on isolated double wells have shown that states form avoided crossings when coupled resonantly, resulting in a ramp-dependent population of Floquet states [31]. By ramping up K_0 away from resonance and, then, tuning $U_{\mathrm{load}} \rightarrow U_{\mathrm{final}}$ in the driven system (green circles), $\mathcal{D}$ gets closer to the undriven values (blue squares). Thus, this driving protocol is suitable for realizing a many-body state with effective attractive interactions. In contrast, for the other driving scheme (red diamonds), the level of $\mathcal{D}$ is equivalent for repulsive and attractive effective interactions. Similar to the off-resonant case, we observe a decrease in $\mathcal{D}$ for long timescales ($\tau_{\mathrm{ramp}} > 0.1$ s), even in the undriven lattice. Since all three schemes show a similar loss of $\mathcal{D}$, heating seems to be unrelated to the drive. In addition, for 1 s modulation time, we observe atom loss in the driven system.

We have seen that deviations from the undriven system arise when the modulation leads to additional atom loss. In our measurements, these losses have been minimized by a smart choice of geometry, namely a hexagonal lattice with tunable band gaps. In general, for a noninteracting system, atom loss can be caused by resonant coupling to energetically higher bands in single- or multiphoton processes [54–59]. As a result, larger band gaps and less dispersive higher bands broaden the frequency window suitable for a Floquet system and reduce the atom loss [58]. By using an anisotropic lattice along the modulation direction ($t_x \neq t_w$), we tune the band gap and dispersion of higher bands, while the bandwidth of the lowest band is kept on a similar level [see Figs. 4(a) and 4(b)]. Figure 4(c) shows the remaining number of atoms after modulating for 1 s at various frequencies with $K_0 = 1.43(2)$. We compare the loss for the hexagonal lattice used in the measurements of the evolution of $\mathcal{D}$ with a dimerized and simple cubic lattice in the weakly repulsive regime ($U/h = 0.71(2)$ kHz). While the atom loss in the simple cubic lattice is quite severe, a dimerization significantly improves the situation and a minimal loss rate is reached for the hexagonal lattice [60].

To further investigate the role of interactions in the hexagonal lattice, we measure the atom loss at different U

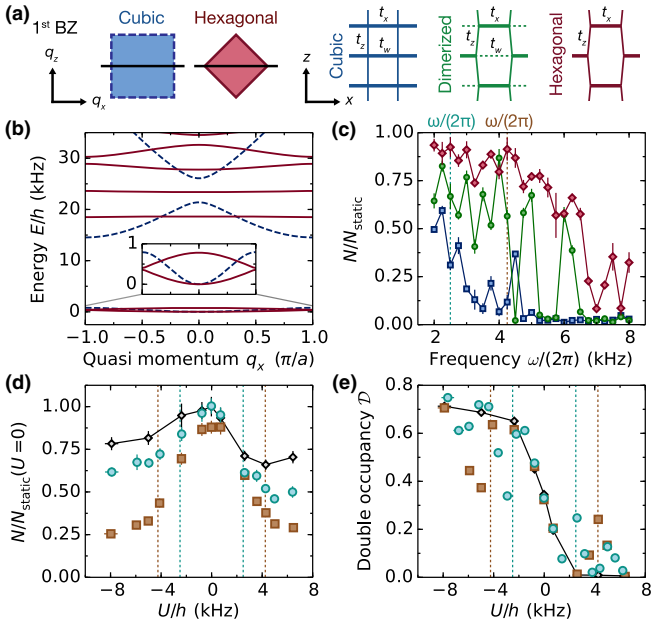

FIG. 4. Minimizing atom loss in driven 3D optical lattices. (a) Schematics of the first Brillouin zone (1st BZ) of the simple cubic (SC, blue) and hexagonal (HC, red) lattices and their real space geometry including an intermediate dimerized (D, green) lattice. All three lattice configurations have $t_x/h \approx 200$ Hz but a different t_w/h [SC: 200(10) Hz, D: 36(2) Hz and HC: < 1 Hz]. (b) Calculated band structure ($q_z = 0$) for the SC (HC) lattice plotted in blue-dashed (red). The HC lattice allows us to tune the band gap and dispersion of the higher band, while the bandwidth of the lowest band remains similar compared to the SC lattice (see inset). (c) Remaining fraction of atoms N/N_{static} when driving for 1 s at fixed $K_0 = 1.43(2)$ for different frequencies $\omega/(2\pi)$ at $U/h = 710(20)$ Hz, where N_{static} is the remaining atom number after holding the system for 1 s in the undriven lattice. The two vertical dashed lines indicate the driving frequencies used in (d) and (e). (d) Normalized atom number $N/N_{\mathrm{static}}(U = 0)$ in the HC lattice after a modulation of 1 s at $K_0 = 1.43(2)$ for two different frequencies $\omega/(2\pi) = 4.25$ kHz (orange) and $\omega/(2\pi) = 2.5$ kHz (cyan) and without drive (black) as a function of U. (e) $\mathcal{D}$ corresponding to the measurements in (d) but for a modulation time of 5 ms. Dashed vertical lines in (d) and (e) correspond to the resonance condition $U = \pm\hbar\omega$. Data points in c(d, e) are the mean and standard error of 3(5) individual measurements at different times within one driving period. Error bars in U result from the uncertainty of the interaction calibration.

when modulating for 1 s [$K_0 = 1.43(2)$] [see Fig. 4(d)]. We compare this data with measurements where the atoms are held in a static lattice for 1 s. In general, atom loss is increased for stronger U, both in the static and driven hexagonal lattice. However, interactions do not introduce new resonant features even though the fraction of double occupancies $\mathcal{D}$ shows the expected reduction (increase) when driving resonantly to the attractive (repulsive) interactions [see Fig. 4(e)].

In conclusion, we have demonstrated the validity of the effective Hamiltonian over several orders of magnitude in

evolution time for near- and off-resonant modulation. Furthermore, our results show that the driven Fermi-Hubbard model can be implemented on realistic experimental timescales, since atom loss and technical heating dominate only after relatively long modulation times. In future work, a direct comparison to theoretical simulations can provide further understanding of driven interacting systems and allow us to investigate Floquet prethermal states [7,10,11,14,17,20]. Moreover, a successful implementation and benchmarking of driven many-body states opens the possibility of investigating the $t-J$ model [61] and correlated hopping systems [24,28,33,62]. In addition, we can extend our technique to complex density dependent tunneling to realize exotic interacting topological systems and dynamical gauge fields [25,63–65].

We thank H. Aoki, J. Coulthard, D. Jaksch, Y. Murakami, and P. Werner for insightful discussions and G. Jotzu for careful reading of the manuscript. We acknowledge Swiss National Science Foundation (Projects No. 169320 and NCCR QSIT), Swiss State Secretary for Education, Research and Innovation Contract No. 15.0019 (QUIC) and ERC Advanced Grant TransQ (Project No. 742579) for funding.

[1] N. Goldman and J. Dalibard, Phys. Rev. X **4**, 031027 (2014).
[2] M. Bukov, L. D'Alessio, and A. Polkovnikov, Adv. Phys. **64**, 139 (2015).
[3] A. Eckardt, Rev. Mod. Phys. **89**, 011004 (2017).
[4] A. Lazarides, A. Das, and R. Moessner, Phys. Rev. E **90**, 012110 (2014).
[5] L. D'Alessio and M. Rigol, Phys. Rev. X **4**, 041048 (2014).
[6] D. Poletti and C. Kollath, Phys. Rev. A **84**, 013615 (2011).
[7] S. A. Weidinger and M. Knap, Sci. Rep. **7**, 45382 (2017).
[8] V. Novičenko, E. Anisimovas, and G. Juzeliunas, Phys. Rev. A **95**, 023615 (2017).
[9] D. A. Abanin, W. De Roeck, and F. Huveneers, Phys. Rev. Lett. **115**, 256803 (2015).
[10] D. A. Abanin, W. De Roeck, W. W. Ho, and F. Huveneers, Phys. Rev. B **95**, 014112 (2017).
[11] M. Bukov, S. Gopalakrishnan, M. Knap, and E. A. Demler, Phys. Rev. Lett. **115**, 205301 (2015).
[12] T. Mori, T. Kuwahara, and K. Saito, Phys. Rev. Lett. **116**, 120401 (2016).
[13] T. Kuwahara, T. Mori, and K. Saito, Ann. Phys. (Amsterdam) **367**, 96 (2016).
[14] E. Canovi, M. Kollar, and M. Eckstein, Phys. Rev. E **93**, 012130 (2016).
[15] F. Peronaci, M. Schiró, and O. Parcollet, Phys. Rev. Lett. **120**, 197601 (2018).
[16] R. Moessner and S. L. Sondhi, Nat. Phys. **13**, 424 (2017).
[17] A. Herrmann, Y. Murakami, M. Eckstein, and P. Werner, Europhys. Lett. **120**, 57001 (2017).
[18] A. Eckardt and E. Anisimovas, New J. Phys. **17**, 093039 (2015).
[19] T. Bilitewski and N. R. Cooper, Phys. Rev. A **91**, 033601 (2015).
[20] M. Bukov, M. Heyl, D. A. Huse, and A. Polkovnikov, Phys. Rev. B **93**, 155132 (2016).
[21] M. Reitter, J. Näger, K. Wintersperger, C. Sträter, I. Bloch, A. Eckardt, and U. Schneider, Phys. Rev. Lett. **119**, 200402 (2017).
[22] C. V. Parker, L.-C. Ha, and C. Chin, Nat. Phys. **9**, 769 (2013).
[23] M. Aidelsburger, M. Atala, S. Nascimbène, S. Trotzky, Y.-A. Chen, and I. Bloch, Appl. Phys. B **113**, 1 (2013).
[24] M. Di Liberto, C. E. Creffield, G. I. Japaridze, and C. Morais Smith, Phys. Rev. A **89**, 013624 (2014).
[25] A. Bermudez and D. Porras, New J. Phys. **17**, 103021 (2015).
[26] N. Goldman, J. Dalibard, M. Aidelsburger, and N. R. Cooper, Phys. Rev. A **91**, 033632 (2015).
[27] J. H. Mentink, K. Balzer, and M. Eckstein, Nat. Commun. **6**, 6708 (2015).
[28] F. Meinert, M. J. Mark, K. Lauber, A. J. Daley, and H.-C. Nägerl, Phys. Rev. Lett. **116**, 205301 (2016).
[29] S. Kitamura and H. Aoki, Phys. Rev. B **94**, 174503 (2016).
[30] J. R. Coulthard, S. R. Clark, S. Al-Assam, A. Cavalleri, and D. Jaksch, Phys. Rev. B **96**, 085104 (2017).
[31] R. Desbuquois, M. Messer, F. Görg, K. Sandholzer, G. Jotzu, and T. Esslinger, Phys. Rev. A **96**, 053602 (2017).
[32] M. E. Tai, A. Lukin, M. Rispoli, R. Schittko, T. Menke, D. Borgnia, P. M. Preiss, F. Grusdt, A. M. Kaufman, and M. Greiner, Nature (London) **546**, 519 (2017).
[33] F. Görg, M. Messer, K. Sandholzer, G. Jotzu, R. Desbuquois, and T. Esslinger, Nature (London) **553**, 481 (2018).
[34] Y. Baum, E. P. L. van Nieuwenburg, and G. Refael, SciPost Phys. **5**, 017 (2018).
[35] K. M. Fujiwara, K. Singh, Z. A. Geiger, R. Senaratne, S. Rajagopal, M. Lipatov, and D. M. Weld, arXiv:1806.07858.
[36] M. Genske and A. Rosch, Phys. Rev. A **92**, 062108 (2015).
[37] S. Lellouch, M. Bukov, E. Demler, and N. Goldman, Phys. Rev. X **7**, 021015 (2017).
[38] Y. Wang, M. Claassen, B. Moritz, and T. P. Devereaux, Phys. Rev. B **96**, 235142 (2017).
[39] A. Keles, E. Zhao, and W. V. Liu, Phys. Rev. A **95**, 063619 (2017).
[40] T. Qin and W. Hofstetter, Phys. Rev. B **97**, 125115 (2018).
[41] L. Tarruell, D. Greif, T. Uehlinger, G. Jotzu, and T. Esslinger, Nature (London) **483**, 302 (2012).
[42] See Supplemental Material at http://link.aps.org/supplemental/10.1103/PhysRevLett.121.233603 for the preparation protocols and experimental parameters.
[43] R. Jördens, L. Tarruell, D. Greif, T. Uehlinger, N. Strohmaier, H. Moritz, T. Esslinger, L. De Leo, C. Kollath, A. Georges, V. Scarola, L. Pollet, E. Burovski, E. Kozik, and M. Troyer, Phys. Rev. Lett. **104**, 180401 (2010).
[44] T. Uehlinger, G. Jotzu, M. Messer, D. Greif, W. Hofstetter, U. Bissbort, and T. Esslinger, Phys. Rev. Lett. **111**, 185307 (2013).
[45] A. Eckardt, C. Weiss, and M. Holthaus, Phys. Rev. Lett. **95**, 260404 (2005).
[46] H. Lignier, C. Sias, D. Ciampini, Y. Singh, A. Zenesini, O. Morsch, and E. Arimondo, Phys. Rev. Lett. **99**, 220403 (2007).

[47] A. Zenesini, H. Lignier, D. Ciampini, O. Morsch, and E. Arimondo, Phys. Rev. Lett. **102**, 100403 (2009).
[48] The driving primarily addresses the bonds along the x direction but, also, slightly modifies the bonds along z (see Supplemental Material [42] for more information).
[49] A. P. Itin and M. I. Katsnelson, Phys. Rev. Lett. **115**, 075301 (2015).
[50] M. Bukov, M. Kolodrubetz, and A. Polkovnikov, Phys. Rev. Lett. **116**, 125301 (2016).
[51] R. Ma, M. E. Tai, P. M. Preiss, W. S. Bakr, J. Simon, and M. Greiner, Phys. Rev. Lett. **107**, 095301 (2011).
[52] Y.-A. Chen, S. Nascimbène, M. Aidelsburger, M. Atala, S. Trotzky, and I. Bloch, Phys. Rev. Lett. **107**, 210405 (2011).
[53] M. Eckstein, J. H. Mentink, and P. Werner, arXiv:1703.03269.
[54] M. Weinberg, C. Ölschläger, C. Sträter, S. Prelle, A. Eckardt, K. Sengstock, and J. Simonet, Phys. Rev. A **92**, 043621 (2015).
[55] G. Jotzu, M. Messer, F. Görg, D. Greif, R. Desbuquois, and T. Esslinger, Phys. Rev. Lett. **115**, 073002 (2015).
[56] C. Sträter and A. Eckardt, Z. Naturforsch. A **71**, 909 (2016).
[57] A. Quelle and C. M. Smith, Phys. Rev. E **96**, 052105 (2017).
[58] G. Sun and A. Eckardt, arXiv:1805.02443.
[59] N. Fläschner, M. Tarnowski, B. S. Rem, D. Vogel, K. Sengstock, and C. Weitenberg, Phys. Rev. A **97**, 051601 (2018).
[60] We find the dispersion and band gaps along the driving direction to be most relevant for atom loss.
[61] J. R. Coulthard, S. R. Clark, and D. Jaksch, Phys. Rev. B **98**, 035116 (2018).
[62] Á. Rapp, X. Deng, and L. Santos, Phys. Rev. Lett. **109**, 203005 (2012).
[63] T. Keilmann, S. Lanzmich, I. Mcculloch, and M. Roncaglia, Nat. Commun. **2**, 361 (2011).
[64] N. Goldman, G. Juzeliunas, P. Öhberg, and I. B. Spielman, Rep. Prog. Phys. **77**, 126401 (2014).
[65] S. Greschner, G. Sun, D. Poletti, and L. Santos, Phys. Rev. Lett. **113**, 215303 (2014).